Atmos. Chem. Phys. Discuss., 9, 22223–22269, 2009
www.atmos-chem-phys-discuss.net/9/22223/2009/

Atmospheric Chemistry and Physics Discussions

This discussion paper is/has been under review for the journal *Atmospheric Chemistry and Physics (ACP)*. Please refer to the corresponding final paper in *ACP* if available.

Spatio-temporal aerosol optical characteristics over the Arabian Sea during the pre monsoon season

D. G. Kaskaoutis[1], M. C. R. Kalapureddy[2], P. C. S. Devara[2], P. G. Kosmopoulos[3], P. T. Nastos[3], K. Krishna Moorthy[4], and H. D. Kambezidis[1]

[1]Atmospheric Research Team, Institute for Environmental Research and Sustainable Development, National Observatory of Athens, Lofos Nymphon, P.O. Box 20048, 11810 Athens, Greece
[2]Physical Meteorology and Aerology Div., Indian Institute of Tropical Meteorology, Pahan, Pune 411008, India
[3]Department of Geology and Geoenvironment, University of Athens, University campus 15784 Athens, Greece
[4]Space Physics Laboratory, Vikram Sarabhai Space Centre, Trivandrum 695022, India

Received: 27 February 2009 – Accepted: 16 September 2009 – Published: 21 October 2009

Correspondence to: M. C. R. Kalapureddy (kalapureddy1@gmail.com)

Published by Copernicus Publications on behalf of the European Geosciences Union.

Abstract

Ship-borne Aerosol Optical Depth (AOD) measurements obtained by a sunphotometer have been used to retrieve the Ångström wavelength exponent (α). These measurements were obtained in the Arabian Sea (AS), where the surrounded arid-region influence is expected, during the pre-monsoon season. Spectral variation of α is typically considered in this study. It is found that the polynomial fit becomes more accurate in the wavelength band 340–1020 nm rather than the 340–870 nm. The coarse-mode (positive curvature in the ln τ_α vs ln λ) aerosols are mainly depicted in the Northern part of the AS closely associated with the nearby arid areas and fine-mode aerosols are mainly observed over the far and coastal AS regions. In the study period the mean AOD at 500 nm is 0.246±0.114 and the $\alpha_{340-1020}$ is 0.904±0.186. The $\alpha_{340-870}$ exhibits similar values (0.924±0.179), while significant differences revealed for the constant terms of the polynomial fit (a_1 and a_2) proportionally to the wavelength band used for their determination. Observed day-to-day variability in the aerosol load and optical properties are direct consequence of the local winds and air-mass trajectories along with the position of the ship.

1 Introduction

The characterization of aerosol particles and the spectral dependence of their extinctions are very important as they strongly influence the radiative properties (single scattering albedo, asymmetry factor, refractive index) in the atmosphere (El-Metwally et al., 2008). The Arabian Sea region has a unique weather pattern in view of the Indian monsoon and the associated winds that reverse direction seasonally. It is a location where the pristine air masses from the Southern Indian Ocean (IO) and the polluted air from Asia meet during winter and spring season, providing a very interesting area for aerosol studies (Ramanathan et al., 2001). Moreover, the investigation of the aerosols over oceans is important from the standpoint of understanding their anthropogenic

ACPD

9, 22223–22269, 2009

and natural impacts as well as in estimating their contribution to radiative forcing (e.g. Haywood et al., 1999; Satheesh et al., 2006a). However, the high spatio-temporal variability and limited measurements of the aerosol physical and optical properties over oceanic regions makes it difficult to understand their impact on weather modification and hence climate change. Due to these reasons the oceanic regions, surrounding India, have always been the subject of importance and investigating extensively by various experimental campaigns.

Despite the airmass origin and the local and regional meteorology, the aerosol load and spatial distribution around the AS region are highly variable from day to interanual scales and strongly affected by the El Nino-La Nina patterns and the location of the ITCZ (e.g. Moorthy and Satheesh, 2000; Ramachandran and Jayaraman, 2002; Li and Ramanathan, 2002). It has been noticed higher AODs and steeper gradients over the northern part of the AS which is mainly attributed to the advected mineral dust from west Asia and also shown a large effect on the radiative forcing in the region (e.g. Satheesh et al., 2006a). Larger sea-salt contribution to the AOD found over AS, especially over the southern AS, during the summer monsoon season which is directly associated with the stronger sea-surface winds (Satheesh et al., 2006b). The chemical species that contribute significantly to the AODs over the AS noticed to be sulfate, sea salt and nitrate, potassium, organics, Black Carbon (BC), dust, fly ash and ammonium (Savoie et al., 1987; Krishnamurti et al., 1998; Nair et al., 2004; Kumar et al., 2008). Large reduction in BC mass fraction over the AS region found from winter to summer significantly affect the seasonal radiative forcing (Babu et al., 2004). Several earlier estimates of the anthropogenic contribution to mean AOD over the AS and northern Indian Ocean showed large variations from 65% to >90% (Satheesh et al., 1999; Ramachandran 2004b). The total aerosol-mass concentration decreased from as high as about 80 μgm^{-3} near the Indian coast to very low values of only a few tenths of μgm^{-3} over the most distant oceanic regions. The large increase in the small-particle concentration near the coast was also consistent with the corresponding large increase in the Ångström exponent, which increased from 0.2 over the Indian Ocean to about 1.4 near

ACPD
9, 22223–22269, 2009

the Indian coast (Krishnamurti et al., 1998). In the following years we might expect aerosol concentrations in this region to increase in concern with the rapid economic development that is taking place in this region, especially in the Indian subcontinent. Therefore, it needs continuous and systematic efforts to monitor the aerosol field and properties over this region since the knowledge of their effects on the marine environment and in our changing planet is a real challenge.

The Integrated Campaign for Aerosols, gases and Radiation Budget (ICARB) (Moorthy et al., 2008) was conducted in the pre-monsoon season of 2006 over the Bay of Bengal (BoB), IO and AS. In the present study, we use the ICARB campaign ocean segment data over AS during the pre-monsoon season (April-May) of 2006 focusing on the AOD and Ångström exponent spectral variation and curvature, which can constitute the basis for aerosol type discrimination over the area. The results are examined against total and size-resolved aerosol-mass concentration measured simultaneously in the marine atmospheric boundary layer (MABL). In addition, we also discuss the errors and the uncertainties revealed in the estimation of the curvature of the lnAOD vs lnλ line over oceanic regions, where the AOD is relatively low. The inclusion of two wavelength bands for characterizing the aerosol optical properties reveals the effects of the wavelength in the aerosol microphysical properties, which can be significant over oceanic regions with a very inhomogeneous aerosol field. These investigations are the very first showing the spatial distribution of the AOD curvature over the AS region.

2 Data collection

The whole set of oceanic segment measurements during the ICARB campaign was conducted onboard the Oceanographic Research Vessel Sagar Kanya. AS region was covered in the second leg (SK223B) of the campaign started from the port of Kochi (on the west coast of India, Fig. 1) on 18 April and ended after 24 days at Goa port (15.4° N, 73.8° E) on 11 May. It reached its farthest west point (14° N, 58° E) on 22 April and 3 May 2006. The track of the ship cruise was designed in such a way that the maximum

ACPD
9, 22223–22269, 2009

possible marine regions in the AS to be covered during the period of observations (see Fig. 1). The points on the track show the position of the ship at 05:30 UTC on each day obtained from a GPS receiver; the dates being identified beside with suffix A for April and My for May. The intense field phase of ICARB in the AS region covered the longitudinal sector 58° E–76° E with a latitudinal coverage from 8° N to 22° N.

High temporal resolution (~10 min) observations of direct-beam solar radiation were made using the hand-held sunphotometer (Microtops-II, Solar Light Company, USA). This sunphotometer provides the AOD at 6 channels (340, 440, 500, 675, 870, and 1020 nm with a FWHM of 5 to 10 nm), columnar water vapor and ozone derived from instantaneous solar flux measurements using its internal calibration. The field-of-view (FOV) of the Microtops-II is 2.5°. A typical error in the AOD estimation from the Microtops-II measurements is ±0.03 (Morys et al., 2001).

It should be noted that Shaw (1980) reported anomalous weak absorption at 1010 nm, possibly from water vapor, since the extinction at this wavelength increased when column water vapor (PW) increased. Eck et al. (2001) showed, using water vapor line spectrographic parameters as given by Giver et al. (2000), that at 1020 nm computed water vapor optical depth of ~0.009 for a tropical atmosphere with 4.0 cm of PW. There is another possible uncertainty associated with the 1020 nm channel due to the temperature-sensitivity of silicon detector at this wavelength (~0.002/°C) (Holben et al., 1998). This remains a source of uncertainty at AOD_{1020} that may not exist for the other wavelengths where the detector temperature sensitivity is insignificant. Unfortunately, the Microtops II algorithm does not take into account the temperature sensitivity of the silicon photodiodes. This is probably a problem only during very clear conditions when the AOD is very small. However this uncertainty of AOD_{1020} has minimized by keeping the Microtops II in shaded area after each observation to maintain it with the near same environmental temperature. In the present study, PW is observed to be 2.22±0.44 cm (Kalapureddy et al., 2008). So, the possible water vapor absorption effects at 1020 nm have not been considered in this study.

During the campaign three sets of measurements were collected in quick succession

ACPD
9, 22223–22269, 2009

(∼1 min) at every 10-min time interval, to avoid any possible errors due to sun pointing on a moving platform. If the three measurements were not close in magnitude, thus producing large differences (above 5%) in the AODs, the dataset was rejected from further analysis. Great attention was given to choose which of the three measurements in each 10-min interval should be retained for further analysis. Thus, they were retained for further analysis that AOD estimation of the three derived, which gave the best second-order polynomial fit to the $\ln\tau_\alpha$ vs $\ln\lambda$ data points (Eck et al., 1999; Kaskaoutis et al., 2007a); the other two AODs were discarded. The fit was controlled by the highest R^2 associated with it. In case the errors were close to each other, additional criteria were followed, such as the AOD values not to change significantly from the previous measurements or the spectral AOD variation to have as less spectral curvature as possible. Furthermore, data recorded around cloud passage or near the FOV of the instrument were not considered for analysis (Kalapureddy and Devara, 2008). After this procedure 1268 out of 4443 spectral measurements remained for further analysis. Thus, depending on the sky conditions the number of available data varies from 23, on 19 April to 69 on 1 May.

3 Climatology of the area

The climatology of the area is mainly dictated by the presence of monsoon, which divides the year into four periods. The mean winds are weak and predominantly from the north/northeastern direction during the winter monsoon season (December to March) where advection from the Indian continent is important. In the summer monsoon season (June to September) the mean winds are strong (10 to 15 ms^{-1}) and mainly westerly/southwesterly favoring the advection from oceanic regions and western land areas. During March-June, it is hot and dry in the Africa, Arabian Peninsula and the Iranian desert regions, while the westerly winds carry significant amount of dust particles over Northern AS (Moorthy and Satheesh, 2000; Li and Ramanathan, 2002; Moorthy et al., 2005). A complete analysis of the wind pattern and rainfall over AS has been reported

ACPD
9, 22223–22269, 2009

in Moorthy and Satheesh (2000). During the ICARB campaign, winds over the AS are mainly from the northwestern sector with an average speed of about 6–9 ms^{-1} (Kalapureddy and Devara, 2008). Precipitation was almost absent throughout the cruise period. A low level anticyclone centered over the central AS was the cause for the northwesterly winds. The mean synoptic wind pattern (derived from the NCEP-NCAR reanalysis data) at 850 hPa over AS during ICARB comprised of strong westerlies over the northern part AS and weaker northerly/northeasterly over the southern part of AS (Nair et al., 2008).

4 Theoretical background and methodology

The spectral dependence of AOD is frequently parameterized by the Ångström exponent α, which is computed from the Ångström's (1961) empirical formula:

$$\tau_{\alpha\lambda} = \beta\lambda^{-\alpha} \quad (1)$$

where β represents the aerosol load in the atmosphere and is equal to the AOD at 1 μm, while α contains information about the nature of the aerosol particles present in the atmosphere and is a good indicator of their size or of the fraction of the fine-mode aerosols in the atmosphere (Schuster et al., 2006).

The validity of the Ångström formula assumes the validity of the Junge power law (Junge, 1955) for the aerosol-size distribution, especially in range from 0.05 to 10 μm, where significant extinction takes place and the spectral variation of the refractive index does not impose significant variations on the Mie extinction factor. The Junge power law introduces a lognormal aerosol-size distribution, which is far away from the bimodal distribution of the aerosols in the atmosphere (Eck et al., 1999). Consequently the Ångström formula is not always valid for all environments and especially in an extended wavelength range. Therefore, the Ångström formula is, in general, well fitted to the AOD values at the shorter or longer wavelengths; when the spectral range is extended, significant uncertainties may reveal (Kaskaoutis and Kambezidis, 2006). This

ACPD
9, 22223–22269, 2009

fact leads to the departure from linearity when the spectral AOD is plotted in logarithmic coordinates (Eck et al., 1999; Kaskaoutis et al., 2007a). Due to this discrepancy, very differing α values can be obtained for different wavelength ranges (Reid et al., 1999; Kaskaoutis et al., 2007a). Under these conditions, a curvature is observed in the $\ln\tau_\alpha$ vs $\ln\lambda$ data points, which contains useful information about the aerosol type and size distribution (King and Byrne, 1976; Eck et al., 1999; O' Neill et al., 2001). Therefore, a second order polynomial fit to the $\ln\tau_\alpha$ vs $\ln\lambda$ data can give a greater accuracy:

$$\ln\tau_\alpha = a_2(\ln\lambda)^2 + a_1\ln\lambda + a_o \quad (2)$$

where the coefficient a_2 accounts for the curvature often observed in sunphotometric measurements (Eck et al., 1999; Kaskaoutis et al., 2007a).

The AOD values at each wavelength are obtained from the direct-beam irradiance measurements via the Bouguer-Beer law. Extensive analysis of the errors retrieved via this methodology is described in Kaskaoutis and Kambezidis (2006). The ozone optical depth was omitted in the derivation of the AOD, since its contribution to the total atmospheric optical depth can be significant under low turbidities. However, no correction was taken into account due to the trace-gases optical depth assuming it negligible over the oceanic regions (Kaskaoutis et al., 2007b). The Ångström parameters, α and β, were calculated via the least-squares method in the spectral ranges 340–1020 nm and 340–870 nm. According to the analysis performed by Kaskaoutis and Kambezidis (2008), this method is the least imprecise and wavelength dependent for the calculation of the Ångström parameters. The second-order polynomial fit (Eq. 2) was also applied to the AOD values at six wavelengths (340, 440, 500, 675, 870 and 1020 nm), although three of them were just sufficient for this computation. The same fit was also applied excluding the 1020-nm wavelength in order to investigate the differences in the retrieved parameters.

ACPD
9, 22223–22269, 2009

5 Estimation of errors and uncertainties

Before analyzing the temporal and spatial variation of the aerosol optical properties over AS a detailed analysis is given regarding the errors and the uncertainties of the 2nd order fits to the spectral AOD data. An account of the typical errors in the estimation of the a_1 and a_2 (Eq. 2) as well as some relationships between the computed coefficients, are provided in this section. The second-order polynomial fit to the $\ln\tau_\alpha$ vs $\ln\lambda$ data has been shown to provide good agreement with measured AODs, involving differences of the order of the uncertainty in the measurements, opposite to the linear fit to the $\ln\tau_\alpha$ vs $\ln\lambda$, which yields significant differences with measured AODs (Eck et al., 2001; Kaskaoutis and Kambezidis, 2006). However, this is not always valid over oceanic regions with relative low AODs. Figure 2 shows the correlation of the typical errors in a_1 and a_2 computed in the two spectral bands, 340–1020 nm and 340–870 nm with the AOD at 500 nm (AOD_{500}). Large errors in the computed coefficients are seen for low AOD_{500} values (<0.2) also exhibiting large variation. Nevertheless, as the atmospheric turbidity increases (AOD_{500}>0.3) the error in the estimates decreases dramatically. This feature is common in sunphotometric measurements, since has been observed in many studies (see Kaskaoutis et al., 2006b and references therein) and is attributed to the higher scatter of the spectral AODs under low turbidity conditions.

The day-to-day variation of the errors in a_1 and a_2 is presented in Fig. 3. Large errors occurred in a_1 and a_2 in the period from 21 to 24 April and, especially, from 1 to 4 May, closely associated with low AOD values as will be seen in the following since the ship was cruising at the far AS. On the other hand, low errors are presented in the period from 25 to 27 April, the ship was near to Indian coast and from 6 to 10 May (ship in the northern AS), both closely associated with high AODs. When the spectral band 340–1020 nm was used for the polynomial fit, the errors were significantly lower in almost all cases, exhibiting mean values of $erra_1$=0.295±0.182 and $erra_2$=0.273±0.166 against those of $erra_1$=0.495±0.284 and $erra_2$=0.380±0.229 computed when the 340–870 nm was considered. It was found that the highest errors in both a_1 and a_2 are found on

ACPD
9, 22223–22269, 2009

days or cases where the curvature (a_2) in the the $\ln\tau_\alpha$ vs $\ln\lambda$ relation was high and, more specifically negative, indicative of the presence of fine-mode aerosols. As will be seen in the following, on the days of high errors (21-24 April and 1–4 May), when the ship was cruising in the far AS, the α values were the highest; on the other hand significant presence of coarse-mode aerosols in the northern part of the AS (29 April and 6–10 May) results in a bimodal aerosol size distribution where the linear and the second order polynomial fits present higher accuracy. To this respect, the correlations between the errors in a_1 and a_2 with the Ångström exponent α for each of the two spectral bands used are strongly positive. The following relations hold:

$$\mathrm{erra}_2 = 0.424\alpha - 0.095,\ R^2 = 0.28\ (340-1020\,\mathrm{nm}) \quad (3)$$

$$\mathrm{erra}_1 = 0.457\alpha - 0.102,\ R^2 = 0.28\ (340-1020\,\mathrm{nm}) \quad (4)$$

$$\mathrm{erra}_2 = 0.678\alpha - 0.214,\ R^2 = 0.32\ (340-870\,\mathrm{nm}) \quad (5)$$

$$\mathrm{erra}_1 = 0.838\alpha - 0.264,\ R^2 = 0.32\ (340-870\,\mathrm{nm}) \quad (6)$$

These results are in general agreement with those reported by previous studies (Eck et al., 1999; Kaskaoutis et al., 2007a) that showed that the 2nd order polynomial fit presents larger uncertainties for large fine-mode aerosol fraction, while the fit seems to be more accurate for bimodal aerosol size distributions with a large coarse-mode fraction. In general, Fig. 3 showed that the use of the 340–1020 nm band, instead of the 340–870 nm one, seems to be more appropriate for the aerosol retrievals. This fact also indicates the great effort and attention spent on the accuracy of the AOD_{1020}.

Through the Ångström's formula (Eq. 1) both coefficients α and β are assumed independent from each other and from the wavelength interval used for their determination. However, it is well known from numerous publications (e.g. the recent study by Kaskaoutis and Kambezidis, 2008) that both parameters depend on wavelength. When their computation takes place at only shorter or longer wavelengths large uncertainties in the retrievals may occur; these standard errors are reduced when the spectral range

includes both shorter and longer wavelengths. In Fig. 4, α and β calculated in the spectral bands 340–1020 nm and 340–870 nm are correlated. As regards β, the correlation seems to be excellent, since the R^2 value is 0.99, the slope and the internship near to 1 and 0, respectively. As a result, the mean β values are differing in the third decimal. On the other hand, greater uncertainties associated with higher scatter in the correlation plot are shown regarding the α values (R^2=0.85). In some cases the data points are far away from the y=x line exhibiting large differences. The mean α value is larger at the 340–870 nm band, while for higher α values those retrieved at 340–1020 nm band overestimate those at 340–870 nm band. Similar correlations between the α values computed in similar wavelength ranges are presented over four AERONET sites (Kaskaoutis et al., 2007a). However, the study showed that the R^2 value was lower (0.81) in the clean oceanic environment of Nauru compared to that over land sites (R^2 ranged from 0.89 to 0.96). The larger dependence of α values on wavelength is attributed to the fact that this parameter is more sensitive to the spectral AOD distribution (the decreasing rate of AOD with respect to wavelength), while β expresses the AOD at 1 μm by definition.

In Fig. 5, the correlation between α and a_1 (Eqs. 1, 2) is displayed for all the period of measurements using the two spectral intervals. In both figures, as expected, there is an anti-correlation between α and a_1, exhibiting a significant scatter. The scatter is more intense regarding the calculations in the 340–870-nm spectral range where the R^2 value is 0.61. A little higher R^2 value is obtained in the spectral band 340–1020 nm, thus implying better agreement between α and a_1. This fact indicates that the curvature is not so significant and the AOD spectral distribution in logarithmic coordinates approaches linearity (α=$-a_1$). In a previous study (Kaskaoutis et al., 2007a) it was found that the coefficient a_1 is significantly different from α, especially in the maritime and desert aerosol environments of Nauru and Solar Village, respectively. Considering the scatter of the α vs. a_1 data points the role of the curvature in the spectral AOD becomes significant. Consequently, the inclusion of the spectral curvature in the analysis enhances the knowledge about the volume fraction and effective radius of the

fine-mode aerosols at intermediate values of the α (Schuster et al., 2006). From Fig. 5 it is concluded that the use of the 340–1020-nm spectral band for the calculation of the α, a_1 and a_2 values leads to the least imprecise results and with the lowest curvature. This will be further established by the lowest a_2 values in the 340–1020-nm region in the following section.

According to Schuster et al. (2006), the Ångström exponent α is equal to the difference a_2–a_1 to a first approximation. An attempt to verify the validity of this statement is given in Fig. 6. When the curvature is negligible ($a_2 \sim 0$), then $\alpha = -a_1$. The correlations between the Ångström exponent α and the differences a_2–a_1 are shown in Fig. 6 for the spectral ranges 340—1020 nm and 340-870 nm. The two parameters are strongly correlated, as indicated by the R^2 values of 0.96 (340–870 nm) and 0.99 (340–1020 nm). Data points lying onto the y=x line or closely around it indicate the validity of the relation a_2–a_1 = α. According to our analysis, the scattered points (340–870 nm case) correspond to cases where the second-order polynomial fit does not provide high accuracy. These findings are in agreement with those by Schuster et al. (2006) who concluded that the relation $\alpha = a_2 - a_1$ can be considered valid for bimodal size distributions with equivalent contributions from fine- and coarse-mode particles. An overestimation of the a_2–a_1 against α is observed for high α values (upper panel). Schuster et al. (2006) reported that the condition $a_2 - a_1 \geq 2$ corresponds to size distributions dominated by fine-mode aerosols and the $a_2 - a_1 \leq 1$ to size distributions dominated by coarse-mode particles, whereas intermediate values of a_2–a_1 to a wide range of fine-mode fractions. Values greater than 2 are absent in our study, while a significant number of values <1.0 is observed in both graphs. This is expected since the measurements were performed over an oceanic environment where coarse-mode aerosols have a significant fraction.

ACPD
9, 22223–22269, 2009

6 Results

6.1 Daily variation of the aerosol properties

Figure 7 presents the frequency distributions of AOD_{500} and $\alpha_{340-1020}$. The AOD_{500} varies significantly from 0.07 to 0.706 thus implying large variability in aerosol load over the entire AS during the ICARB period. The mean AOD_{500} in AS was found to be 0.246±0.114, which is significantly higher than that observed over open oceanic regions in Pacific and Atlantic oceans (Smirnov et al., 2002). However, the AOD_{500} value over AS is much lower than that observed over BoB (0.36±0.12) during ICARB (Kalapureddy and Devara, 2008), or from previous studies (e.g. Ramachandran, 2004a). The highest frequency of occurrence is depicted at AOD_{500}=0.15, while a significant fraction of the AOD_{500} values is above 0.3. The AOD_{500} frequency distribution appears rather lognormal, with the lower values belonging to the far AS region and the higher ones near the west coast of India and in the northern part of AS, where the effect of the nearby deserts becomes important.

The frequency distribution of the $\alpha_{340-1020}$ approaches the Gaussian distribution as was also observed in the Athens area in May 2005 (Kaskaoutis et al., 2006). This fact implies simultaneous presence of fine- and coarse-mode particles since the $\alpha_{340-1020}$ varies widely from 0.186 to 1.558, exhibiting a mean value of 0.904±0.186. This value agrees with that of 0.86±0.20 over AS and is significantly lower than that (1.21±0.11) over BoB reported by Kalapureddy and Devara (2008) during ICARB. The highest frequency is depicted in the interval 0.8–0.9, while similar frequency of occurrences for high (α>1.1) and low (α<0.7) values is observed. During the 5-year period 1996–2000 the α was 1.50±0.05 over AS, while the β was 0.10 (Ramachandran, 2004a). The large difference in the α values presented in Ramachandran (2004a) may be attributed to different time intervals and the different spatial coverage of the AS region. However, the mean α value in April for the period 1996–2000 was much lower, 1.27±0.07 (Ramachandran, 2004a). The mean α values over Lanai, Nauru and Tahiti in the Pacific Ocean were found to be 0.76, 0.43 and 0.74, respectively. In the Atlantic Ocean on

ACPD
9, 22223–22269, 2009

the Bermuda and Ascension islands, the mean α values were found to be 0.93 and 0.62, respectively (Smirnov et al., 2002). These values are, in general, lower than that over the AS (0.90) calculated in the present study. This indicates the higher influence of the continental anthropogenic aerosols of the Indian subcontinent that dominate the aerosol load over this area. All the studies conducted over the oceanic regions surrounding India (BoB, IO and AS) agree with the higher α values in comparison with those over open oceans.

Figure 8 presents the spectral AOD variation for all the days of the ICARB campaign in the AS region. The AOD at 340 nm (0.315±0.136) is significantly higher than that at longer wavelengths, 0.149±0.075 at 870 nm. On the first days of the cruise, when the ship was nearer to the Indian coast, the spectral AOD variation is larger due to the proximity to the urbanized coast. It is known that aerosols of smaller size contribute more to the AOD at shorter wavelengths and the condensation growth and the coagulation mechanism of submicron aerosols are more efficient in producing accumulation-mode aerosols (Moorthy et al., 1999). These processes are more efficient over coastal regions due to larger amount of hygroscopic components in the coastal aerosol composition. As a direct consequence of the anthropogenic emissions in the industrialized ports of the Indian west coast, the AODs present the highest values in the period from 25 to 27 April, when the ship approaches the coast (Fig. 1). Another significant aspect is the low AODs from 1 to 4 May, when the ship was far away from land. It is seen that over the entire study area the AODs at the shorter wavelengths are ~3 times higher than those measured at the longer ones, indicating the dominance of smaller size aerosols over AS. The western coastal belt of India is densely populated, urbanized and industrialized. It has 5 major ports (from north to south Kandla, Mumbai, Goa, Mangalore and Kochi, marked in Fig. 1) besides several medium and small fishing harbors. More than 40% of the Indian population inhabits the coastal belt of >7500 km length. The effluents from the anthropogenic activities from these regions can contribute to fine- and accumulation-mode aerosols through secondary production mechanisms (condensation, coagulation, and gas-to-particle conversion) in the warm

ACPD
9, 22223–22269, 2009

and humid tropical environment (Moorthy et al., 2005, Babu et al., 2008). On the other hand, on 29 April and on the last days of the cruise the AODs at longer wavelengths are comparable in magnitude with those of 25–27 April. However, the shorter wavelengths AODs are much lower, thus indicating aerosol presence of different origin and composition than the previous ones. As will be shown in the following these aerosols are mainly of desert origin.

The day-to-day variation of the α values computed in the spectral bands 340–1020 nm and 340–870 nm is shown in Fig. 9. The two α values exhibit similar day-to-day variability and their mean values and standard deviations are 0.904±0.186 for 340–1020 and 0.924±0.179 for 340–870. Satheesh et al. (2006a) also found lower α values determined in the spectral band 380–1025 nm compared to those in 380–870 nm. This means that as the wavelength region used for α determination shifts towards shorter wavelengths higher α values are observed, a fact that implies a convex-type curve in the $\ln\tau_\alpha$ vs $\ln\lambda$ relationship, characteristic of aerosols with significant fraction of coarse-mode particles (Eck et al., 1999; Schuster et al., 2006; Kaskaoutis et al., 2007a). This is more pronounced on 29 April and from 6 to 10 May, where the α values are lower, indicative of the presence of coarse-mode aerosols. In contrast, from 1 to 4 May (large α values) the $\alpha_{340-1020}$ seems to be larger than that at 340–870 nm, implying a concave-type curve, where the α values become larger as the wavelength interval includes longer wavelengths (Eck et al., 1999; Schuster et al., 2006; Kaskaoutis et al., 2007a). Due to the bimodal aerosol-size distribution, very different values of α were calculated in different wavelength intervals due to the significant wavelength dependence of the Ångström exponent. Almost a three-fold increase (from 0.5 to 1.5) in the value of α was observed over AS when the wavelength interval changed from shorter (340–440 nm) to longer (675–870 nm) wavelengths (Kalapureddy and Devara, 2008). The t-statistic test between the two sets of α values showed that the mean values are statistically insignificant at the 95% confidence level. As previously noted on the first few days of the cruise when the ship was near the coast, the α values were high (above 1.0). The same feature was repeated between 1 and 4 May when the ship was in the far AS. It is

rather strange to observe such high α values over an oceanic environment, but it was found that on those days the air masses came from continental India and the winds were rather low (below 5 ms^{-1}) not favoring the production of marine aerosols. Therefore, with the absence of intense sea-surface winds and the absence of air masses originating from the arid landscapes surrounding AS from north and west, the aerosol loading over the area is mainly dominated by small anthropogenic components, thus explaining the relative high α values. In contrast, on 29 April and in the period 6–10 May, the α values were rather low indicating significant contribution of coarse-mode particles in the aerosol burden. On these days, the research vessel was in the northern part of the AS and under the continental influence of the nearby arid landscapes. The day-to-day variability in α values over AS could be due to both variations in the aerosol emissions from the Indian subcontinent and the variability in the meteorological conditions (winds and relative humidity). It should be mentioned that the monsoon surface winds may produce large sea-spray aerosols over the adjoining sea surface; the marine aerosols so produced may have large-size dominance.

The coefficients a_1 and a_2 obtained by the polynomial fit (Eq. 2) in the AOD values using the spectral bands 340–1020 nm and 340–870 nm are shown in Fig. 10. Significant daily variability was observed in both a_1 and a_2 values (Fig. 10) with large peaks and gaps. Significant differences can also be observed even in a few (10–20) minute time interval, since the a_1 and a_2 values are very sensitive to any change in the AOD value at any wavelength. In both figures the a_2 values are negative in the majority of the cases (65% for 340–1020 nm and 81% for 340–870 nm) indicating a concave type curve in the $\ln\tau_\alpha$ vs $\ln\lambda$ relation. This type of curve implies the presence of significant amount of fine-mode aerosols in the atmosphere (Eck et al., 1999). Similar negative curvatures are also found over a tropical coastal Indian station, Visakhapatnam, during the summer monsoon period (Madhavan et al., 2008). A significant curvature is observed in the measured AOD spectra almost for all days of the cruise over the AS region. This curvature can be shown by the a_2 values, which can be very large in certain occasions. Since the measurements were conducted on a moving ship, a large

intra-daily and a day-to-day variability in the curvature (a_2 values) and also in a_1 values are expected; these variabilities could be due to the change in the measurement position.

Systematic presence of negative a_2 values, indicative of fine-mode dominating aerosols, is observed on certain days (21 to 24 April and 1 to 4 May), when the research vessel was in the far AS region. Furthermore, both figures show the presence of a_2 values close to 0 on days when the ship was close to the west Indian coast (18–19 and 25–27 April), thus indicating a bimodal aerosol size distribution with nearly similar contribution of fine and coarse particles. On the other hand, both figures reveal the presence of positive a_2 values on 29 April and on the last days of the cruise when the ship was in the northern AS region indicative of the presence of significant fraction of coarse desert-dust aerosols. Previous studies using measurements (Eck et al., 1999; Kaskaoutis et al., 2007a) or theoretical approaches (Schuster et al., 2006) have shown that the curvature is larger (more negative a_2 values) in cases with significant fraction of fine-mode aerosols, becoming negligible (close to zero or even positive a_2 values) in atmospheres dominated by bimodal aerosol size distributions or coarse-mode particles. These results seem to be in close agreement with those observed over the AS region. The sensitivity of the a_1 and a_2 values to the AOD spectral distribution and the small variability of the AOD values is verified from the large range in both a_1 and a_2. Thus, the a_1 varies widely from −3.529 to 0.139 (340–1020 nm) and from −2.596 to 0.459 (340–870 nm). The respective a_2 values range from −2.303 to 0.927 and from −1.176 to 0.769. In general, the mean a_2 values (−0.127±0.315) are lower in the spectral range 340–1020 nm thus implying less curvature, on average, compared to those computed without the AOD_{1020} value (0.198±0.272). Assuming negligible the curvature for $-0.1<a_2<0.1$ it was found that the 38.8% of the cases lie within this limit when the 340–1020 nm band was used, while the fraction is lower (30.8%) for the band 340–870 nm. These cases are mostly observed in the period 25–27 April and on the last days of the cruise when bimodal aerosol size distributions with intermediate values of α dominate. In these cases (492 for 340–1020 nm) the errors in a_1 and a_2 computations

ACPD
9, 22223–22269, 2009

are much lower (0.232 and 0.215, respectively) than those presented above, Fig. 3. Furthermore, the $\alpha_{340-1020}$ value is 0.844, too close to that of the absolute $a_1 = -0.849$. As regards the 340–870 nm band, the errors in a_1 and a_2 computations assuming the curvature negligible (391 cases) are 0.373 and 0.302, respectively, much lower that the values presented in Fig. 3. The mean $\alpha_{340-870}$ value is 0.816, close to that of the absolute $a_1 = -0.847$. From the above results we can conclude that the use of the 340–1020 nm band seems to be more appropriate since results in lower curvatures, lower uncertainties and better correlations. A direct comparison of these values with those reported by Kaskaoutis et al. (2007a) for four AERONET sites should be avoided due to the large standard deviations in the present analysis. These researchers found a positive mean a_2 at Nauru and Solar Village indicative of the presence of coarse-mode aerosols, i.e. maritime and desert particles, respectively. Furthermore, a_2 values near to zero associated with large standard deviations were found in Alta Floresta and Ispra where both fine- and coarse-mode aerosols dominate depending on the season. Regarding a_1, almost all of its values, except very few cases, are negative, as expected, since $a_1 = -\alpha$ on cases without curvature. However, on certain cases, and especially in the period 1 to 4 May (far AS region), some "unreal" positive a_1 values are observed (Fig. 10). On those days the AODs were the lowest (Fig. 8), while the α values the highest, implying low columnar abundance and predominance of accumulation-mode particles. It is interesting to note that for the central part of AS, around the same area as above, from measurements of total and size-segregated mass concentrations of aerosols in the MABL, Nair et al. (2008) have reported very low aerosol- mass concentration and a relatively high (>0.5) accumulation fraction. They had attributed it to faster subsidence (settling down) of aerosols, particularly of the coarse mode, caused by the strong descent of air masses associated with the strong low-level anticyclone prevailing over the area. The number of positive a_1 values was larger when they were computed in the 340–870-nm band (7 cases) against 5 in the band of 340–1020 nm. However, a significant fraction of positive a_1 values was observed in the clean marine environment of Nauru (Kaskaoutis et al., 2007a). From a detailed analysis it was established that

these (positive) values are obtained in cases that AOD_{1020}>AOD_{870} or when the AODs at the shorter wavelengths are much higher compared to those at the longer ones, thus implying the high α values. The positive a_1 values in the band of 340–870 are mainly attributed to the larger AOD_{870} values instead of the AOD_{675} values, a rather common characteristic in clean marine environments (Kaskaoutis et al., 2007a). However, these cases are very few over AS, a fact that differentiates this environment of a background clean marine one. Also, the nearly absence of "unreal" positive a_1 values shows the accuracy of the AOD retrievals over a moving platform in an oceanic area.

During the pre-monsoon season the dry Indian landscapes along with the anthropogenic activity can drive an injection of significant amount of particulate matter in the atmosphere. These particles can be carried over the oceanic environment by the prevailing northeasterly winds within the boundary layer mainly. The northeast monsoonal low-level flow can transport sulfates, mineral dust and other aerosols from land areas being upwind of AS. This transport may also include fine dust from the Arabian desert whose dust size belonging to the accumulation size regime (Hess et al., 1998). The results showed a relatively complicated aerosol mixture of both anthropogenic pollution and mineral dust along with local maritime aerosols in the AS region. In order to understand the connection between continental emissions and impacts over the AS and IO, it is necessary to focus on the role of the northeast monsoon in the large-scale atmospheric circulation.

6.2 Air-mass trajectories

Air-mass back trajectories ending at the ship location each day on 12:00 UTC at three altitudes, 500, 1500 and 3000 m a.s.l., were calculated by the HYSPLIT model (Draxler and Rolph, 2003) (Fig. 11). The back-trajectory analysis provides a three dimensional (latitude, longitude and height) description of the pathways followed by air masses as a function of time by using the National Center for Environmental Prediction (NCEP) reanalysis wind as input to the model. These trajectories are important to identify the source regions and the transport pathways of the aerosols before they reach the

measurement site. Hence they are helpful in investigation of the aerosol properties and aerosol types.

The 7-day air-mass back trajectories for all the days of the measurements in the central part of AS indicate absence of any significant long-range transport from the adjoining continents, as the air masses seem to come from oceanic origin mainly for the 500-m back trajectories during the cruise days, because the air masses originated and remained within the AS region (Fig. 11a–b). The easterly low-level (1500 m) flow from the Indian subcontinent into the AS can carry pollutants and continental aerosols. It has been seen that sulfates and other continental aerosols are transported thousands of kilometers over AS and IO during the northeast monsoon season (Ramachandran and Jayaraman, 2002). It was found that on the days with relative high α-Ångström values (1–4 May), when the ship was in the far AS, the air masses originated mainly from continental India and some times from Arabia (see Fig. 11c–f). The upper-level flow from the Arabian Peninsula precludes the transport of desert dust to the AS at this time of the year. The transport patterns can be quite different for pollutants and aerosols that penetrate the boundary layer to the free troposphere. The westerly flow in the mid-to-upper troposphere north of about 15° N can transport mineral dust from the Arabian Peninsula to the AS. Aerosol transport from the arid landscapes at 3000 m or 1500 m was detected on 29 April and 5–6 May, when the AOD were high and the α low. High AODs appeared on the last days of the cruise, when the ship was in the northeastern part of the AS; they rather consisted of mixed particles since the air trajectories show the transport of both anthropogenic and natural aerosols. Meteorological studies showed that high aerosol concentrations could be linked to transport from the Indian subcontinent and also from sources in the Middle East and Arabian Peninsula (Moorthy et al., 2005). Although heavier aerosols may reside (via dry deposition) there still remains a strong possibility for the aerosols from Arabia and the other arid and semi-arid regions to make its way to the AS region. The high AOD values presented in the northern part of the AS provide a strong support to this assertion. Furthermore, mineral dust was found to be a substantial component in most of the aerosol samples collected

ACPD
9, 22223–22269, 2009

in AS (Savoie et al., 1987; Nair et al., 2004; Kumar et al., 2008). Analyzing spectral AODs from a network of observatories over Indian mainland during ICARB, Beegum et al. (2008) showed the significant role of transported dust in enhancing AOD and decreasing α over the Indian subcontinent during April and over the northern part of India and the Indo-Gangetic Plains in May.

6.3 Spatial distribution of the aerosol properties

In this section the spatial distribution of the aerosol load and the optical properties over the AS region are presented. Similar AOD and α maps have already been published by Kalapureddy and Devara (2008) for the whole ICARB campaign, including BoB, IO and AS. In the present study these graphs are presented over AS in more detail, while the a_1 and a_2 spatial distributions over the area are presented for the first time. Figure 12 shows the AOD_{500} spatial distribution over the AS. A strong southwest-to-northeast gradient in the AOD_{500} values is revealed since the aerosol load over the northern part of the AS is larger than that of the southern. However, the lowest AOD_{500} values are depicted in the central part of AS (around 13–14° N) on 30 April and 1 May. A similar strong southeast-to-northwest gradient is observed since the aerosol field is larger near the coastal India. Additionally to the latitudinal variation, a significant longitudinal one is observed, since there is a strong gradient of decreasing AOD_{500} values from around the Indian coast towards the far AS. The high AOD_{500} close to the coast arises mainly from the anthropogenic activities over the coastal regions. It is known that the west coastal regions of India are highly urbanized and industrialized. As the anthropogenic aerosols are generally in the submicron size and, for this reason, have longer residence times, they get transported to greater distances over the ocean. Such cases of aerosol and pollution transport from urbanized regions and mineral dust from the arid areas of northwestern India, Iran and Arabia during the pre-monsoon season have been reported from the back-trajectory analysis (Fig. 11). As the distance from the coast increases these aerosols undergo changes in size due to coagulation and condensation; they also extinct over oceanic areas due to the sedi-

mentation and precipitation processes. These processes lead to a decrease in aerosol load and thus AOD becomes lower in the far AS. Ramachandran (2004b) has indicated via the term "scaling distance" the importance of wind speed over the ocean surfaces in altering the aerosol spectral characteristics and the effect it has on the gradients seen in terms of the continental influence. Close to the Indian subcontinent aerosol-mass concentrations were found to range between 21 and 53 $\mu g\,m^{-3}$ (Nair et al., 2004) and were significantly larger than those near the Maldives ($\sim$19 $\mu g\,m^{-3}$) or at the Kaashidhoo Climate Observatory (Ramanathan et al., 2001). As the Sagar Kanya approached the Asian continent in the north AS region where the synoptic winds were mainly northerly/northwesterly originating from the arid landscapes in Iran and Pakistan (Fig. 11), this caused an enhancement in AOD on 7–10 May. It was found that this enhancement could be attributed to the advection of aerosol-burdened continental air over the northern part of the AS. In a previous study, the AOD was found to increase with latitude between equator and 12° N, while over northern AS did not show significant latitudinal variations (Satheesh et al., 2006a). These researchers reported mean AOD values of 0.29±0.12 during the winter monsoon season (November to March) and 0.47±0.14 during the summer monsoon season (April to September). The respective α values were 0.7±0.12 and 0.3±0.08. The differences in AOD spatial distribution between this study and the results of those researchers may mainly be due to the differences in the period and measurements obtained and the fact that the present study does not include data southern than 8° N, where the AOD was significantly lower without strong continental influence (Satheesh et al., 2006a).

The spatial distribution of the $\alpha_{340-1020}$ values over the entire AS region is shown in Fig. 13. The $\alpha_{340-1020}$ values are high (above 1.0) near the coast (18 April) and in the central part of the AS closely associated with the low AOD_{500} values (Fig. 12). It is worth noting that in the far AS the $\alpha_{340-1020}$ values remained high, without showing strong influence from the arid regions of the Arabian Peninsula. In contrast, low $\alpha_{340-1020}$ values are observed in the north part of the AS region, thus indicating the influence of desert-dust particles transported over this region. It is characteristic the

strong south-to-north gradient in $\alpha_{340-1020}$ values around 15–16° N, with $\alpha_{340-1020}$ values above 0.9 in the south and below 0.8 in the north. However, the most common situation is the intermediate values of $\alpha_{340-1020}$ (near to 0.9), indicating a mixed aerosol field over AS from both anthropogenic and natural emissions. This mixed aerosol is also the case near to the Indian coast due to both influences of anthropogenic and natural sources. The anthropogenic emissions seem to play a significant role in the $\alpha_{340-1020}$ values over AS, which are higher than other marine environments in the Pacific and Atlantic. Unlike the other marine regions, where sea-salt aerosols contribute mostly to the total aerosol-mass concentrations, the aerosol chemical composition analysis performed over IO and Kaashidhoo during INDOEX 1999 found that the sea salt contributes only 11% and 17% to the total aerosol loading, respectively, while the anthropogenic aerosol transported from continental India contributes the most (Ramanathan et al., 2001; Satheesh et al., 2002). Furthermore, Satheesh et al. (2006b) found that the sea-salt contribution to the AOD was about 20–30% in the northern AS and 30–40% in the southern. This fact can partly explain the relative high α values over the far AS. The anthropogenic, as well as the dust contribution, is even higher near the coast of AS and in its northern part as has been shown in Nair et al. (2004). It is well known that the northern AS is influenced by the Indian subcontinent and West Asian arid regions, whereas the southern AS and northern IO are influenced by several source regions where the ITCZ has a great impact (Nair et al., 2004; Satheesh et al., 2006a). As a result, the temporal and spatial variations in the spectral dependence of the AOD are indicative of the changes in the aerosol-size distribution mainly due to the different aerosol types and air masses. Extensive measurements over AS from the Minicoy Island (Moorthy and Satheesh, 2000) have shown that the AOD is higher during the summer monsoon season, whereas its spectral variation is higher during winter monsoon season. Thus, the AOD, as well as its spectral dependence, show large temporal variation over specific regions of AS.

The new results provided in the present study are focused on the a_1 and a_2 values obtained from the polynomial fit (Eq. 2) in the two spectral bands. In Fig. 14 (left and

right panels) the spatial distribution of the a_1 values over the AS region is shown for the spectral bands of 340–1020 nm and 340–870,nm, respectively. The maps were constructed utilizing the whole dataset, in order the spatial distribution of the values as well as the differences arisen in either spectral band to be captured. In general, the two maps providing the a_1 values agree to each other. More specifically, large negative a_1 values are depicted in the far and central AS. In the northern part of the AS and along the Indian coast the a_1 values are less negative than those in the far AS. A general disagreement between the a_1 values shown in Fig. 14 is detected in the south AS, where a_1 for 340–1020 nm is less negative than those of 340–870 nm. One should bear in mind that this area is associated with very low AODs and, therefore, the estimated errors may be high. Thus, the inclusion of the AOD_{1020} value in the polynomial fit may produce large differences in the a_1 values. The correlation of the a_1 values in the two spectral bands exhibits large scatter (R^2=0.35), further highlighting the great importance of the wavelength interval used for such computations.

The most important parameter of the polynomial fit is the a_2 value, which presents the curvature of the AOD spectral distribution in logarithmic coordinates and can be used as an additional tool for the aerosol-type discrimination (Kaskaoutis et al., 2007a). The spatial distribution of both a_2 values is shown in Fig. 15 (left and right panels) for the 340–1020 and 340–870 nm, respectively. Positive values of a_2 are indicative of convex-type curves closely associated with coarse-mode particles, while negative curvatures with fine-mode aerosols. The majority of the area is covered with negative a_2 values (in both figures) over most of the southern and central parts of AS, as well as along the Indian coast, closely associated with aerosols having a large fine-mode fraction. On certain occasions, positive a_2 values were also found in the southern part of AS, especially in Fig. 16a. Furthermore, the inclusion of AOD_{1020} in the a_2 retrievals results in larger fraction of positive a_2 values (35%) against 19% for the 340–870 nm case, a scenario that seems to be more likely over an oceanic environment. These positive a_2 values from the 340–1020 nm band against those (negative) from the 340–870 nm are mainly observed near to the Indian coast and in the south AS region.

ACPD
9, 22223–22269, 2009

Therefore, it is concluded that the spectral band used for the a_2 retrievals strongly differentiate the results, as the coefficient of determination between the two sets of a_2 values is low, R^2=0.23. Positive values of the a_2 (in both figures) are depicted in the northern AS, where the high AODs are dominated by coarse-mode aerosols.

7 Discussion

Nair et al. (2008) have investigated on the spatial distribution of the surface mass concentration and the fine-mode mass fraction over AS during ICARB. Their results are in close agreement with those computed in the present study. More specifically, they found a generally low mass concentration of 16.7±7 μgm^{-3}, almost half of that reported in previous campaigns (e.g. INDOEX). The coarse-mode aerosols (radii>1.0 μm) contributed, on average, by 58% to the total mass even in small regions where the accumulation mode was dominant. Furthermore, the fine-mode fraction was 0.42; for 62% of the measurements, it layed within 0.35 and 0.55. In 4% of the total observations this fraction was >0.75 mainly over the regions with negative a_2 values. More specifically, in the central AS, bounded by 65-70° E and 10-15° N, Nair et al. (2008) found that, although the aerosol-mass concentration was quite low (<15 μgm^{-3}), the contribution of accumulation aerosols to the total mass was greater than 50%. This conclusion is close to ours, since in the same area the AOD is low (Fig. 12), the α-Ångström high (Fig. 13) and the a_2 negative (Fig. 15). Nair et al. (2008) also found high values of mass concentration (~30 μgm^{-3}) in the northern AS (64–68° E, 19–22° N), which are mainly attributed to aerosol transport from arid regions of West Asia. The presence of large aerosol load associated with desert particles over this area can be also highlighted in Figs. 12, 13 and 15. Finally, relative high aerosol-mass concentrations (20±7 μgm^{-3}) were measured along the West Indian coast, mainly composed of anthropogenic emissions (Nair et al., 2008). The present results also show increased AOD_{500} values over this region associated with urban/industrial pollution transport over AS. A direct correlation of the results obtained by Nair et al. (2008) at sea level with this study of

ACPD
9, 22223–22269, 2009

the vertical column focusing on the agreement in the spatial distribution of the aerosol optical properties and size distribution constitutes a real challenge.

Aerosols found over the oceans are mainly sea-salt particles, produced by the evaporating water droplets injected into the atmosphere, and wind-blown dust, transported from the surrounding landmasses. Over the pristine oceanic regions the major contribution to the AOD is from sea salt and sulfate from natural sources. The emission strength of these aerosols is dependent strongly on the surface wind speed. Over the northern IO it has been seen that sea salt and sulfate from natural sources contribute less than 20% to the AODs (Ramanathan et al., 2001; Satheesh et al., 2002), while BC, fly ash, dust, organics and anthropogenic sulfate the rest. As mineral dust particles can be transported over long distances, they can contribute significantly to the aerosol mass in the marine atmosphere (Quinn et al., 2002). This contribution is much higher in the northern parts of the AS where the desert-dust aerosol type (high AOD, low α-Ångström, positive a_2) seems to dominate. Even though it is possible that the oceanic environment is less heterogeneous compared to the land one, several studies have shown that the aerosol properties show significant variations, even over reasonably small spatial scales and the spatial changes are distinctly different in the different seasons (Moorthy and Satheesh, 2000; Smirnov et al., 2002). This is mainly due to changes in air-mass types, the impact of advection and transport, and the proximity to continental areas over which the aerosol properties vary. This is true even over the AS and the tropical Indian Ocean (Kalapureddy and Devara, 2008).

8 Conclusions

Ship-borne sunphotometric measurements of AOD and size segregated mass concentration in the MABL over AS were performed during the pre-monsoon season (April-May 2006) in order to shed light in the spatio-temporal heterogeneity. The present study provides an extensive analysis regarding the errors and the uncertainties in computing the aerosol optical properties. It was found that the use of the spectral

band of 340–1020 nm for the polynomial fit gave more accurate results than the respective of 340–870, where the typical errors can be high. The spectral AOD and α-Ångström values exhibited significant day-to-day variations along the ship cruise mainly attributed to the distance of the ship from the main land, the air-mass origin and atmospheric dynamics. The mean AOD_{500} was found to be 0.246±0.114 and the $\alpha_{340-1020}$ 0.904±0.186. In the majority of the cases the coefficient a_2 was negative, thus implying a concave-type curve indicative of the higher presence of fine-mode aerosols. The observed spatial and temporal variation of the AOD and aerosol optical properties indicated the importance of the role of the transport of aerosols that originate from different source regions (air-mass regimes) pertain to AS.

The data presented a strong latitudinal and longitudinal gradient in the AOD and Ångström exponent. The AODs were found to exhibit a steep gradient as the ship moved from the Indian coast towards the pristine oceanic region, with higher values near the coast and nothern part of AS. Very low AOD values were observed in the central part of the AS region. The α-Ångström also exhibited significant spatial variation, with the higher values to be detected near the Indian coast and in the far AS. The anthropogenic and urban activities along the densely populated western coast of India could be attributed to the former; the later arose from the strong vertical descent of rather clean air, associated with low-level mid-ocean anticyclone which lead to faster depletion of coarse-mode particle concentration. Low values of α are associated with coarse-mode arid aerosols were found in north AS. The present study was the very first one providing the spatial distribution of the coefficients a_1 and a_2 over AS even in two spectral bands. A general agreement was found in the spatial distribution of each coefficient determined in different wavelength bands, despite some differences observed in the south AS region. Positive values of a_2, (indicative of coarse-mode aerosols) were mainly observed in the northern AS. Negative a_2 values (fine-mode aerosol abundance) were observed in the central and far AS. In the study region, in addition to the transport of dust from the arid West Asian regions, convex curvature could also arise from the presence of sea-salt particles as the measurements were

ACPD
9, 22223–22269, 2009

conducted over oceanic regions and from well-mixed aerosols with significant contribution of coarse-mode.

The results indicated a relatively complicated aerosol mixture of both industrial pollution and mineral dust. This dictates the need for careful measurements and analysis to discriminate the dominance of specific aerosol types (e.g. anthropogenic aerosols, maritime particles, mineral dust) in the AS. The combination of such particle types is highly variable and makes attribution of the aerosol radiative properties to specific aerosol types difficult to be detected without detailed and precise measurements.

Acknowledgements. The present study was supported and funded by the Geosphere Biosphere program of the Indian Space Research Organization. The authors are gratefully acknowledging the HYSPLIT scientific team providing the air-mass trajectory analysis. Authors thank the Director, IITM for his constant encouragement.

References

Ångström, A. K.: Techniques of determining the Turbidity of the Atmosphere, Tellus, XIII, 214–223, 1961.

Babu, S. S., Moorthy, K. K., and Satheesh, S. K.: Aerosol black carbon over Arabian sea during inter monsoon and summer monsoon seasons, Geophys. Res. Lett., 31, L06104, doi:10.1029/2003GL018716, 2004.

Babu, S. S., Nair, V. S., and Moorthy, K. K.: Seasonal changes in aerosol characteristics over Arabian Sea and their consequence on aerosol short-wave radiative forcing: Results from ARMEX field campaign, J. Atmos. Solar Terr. Phys., 70, 820–834, 2008.

Beegum, N. S., Moorthy, K. K., Nair, V. S. et al.: Characteristics of Spectral Aerosol Optical Depths over India during ICARB, J. Earth Syst. Sci., 117, S1, 303-313, 2008.

Draxler, R. R. and Rolph, G. D.: HYSPLIT (Hybrid single-particle Lagrangian Integrated Trajectory) model, http://www.arl.noaa.gov/ready/hysplit4.html, NOAA Air Resources Laboratory, Silver, Spring, MD, 2003.

Eck, T. F., Holben, B. N., Reid, J. S., Dubovik, O., Smirnov, A., O'Neill, N. T., Slutsker, I., and Kinne, S.: Wavelength dependence of the optical depth of biomass burning, urban, and desert dust aerosols, J. Geophys. Res., 104, 31 333–31 349, 1999.

Eck, T. F., Holben, B. N., Dubovik, O., Smirnov, A., Slutsker, I., Lobert, J. M., and Ramanathan, V.: Column-integrated aerosol optical properties over the Maldives during the northeast monsoon for 1998–2000, J. Geophys. Res., 106, 28 555–28 566, 2001.
El-Metwally, M., Alfaro, S. C., Abdel Wahab, M., and Chatenet, B.: Aerosol characteristics over urban Cairo: Seasonal variations as retrieved from Sun photometer, J. Geophys. Res., 113, D14219, doi:10.1029/2008JD009834, 2008.
Giver, L. P., Chackerian Jr. C., and Varanasi, P.: Visible near-infrared H20 line intensity corrections for HITRAN96J, Quant. Spectrosc. Radiat. Transfer, 66, 101–105, 2000.
Haywood, J. M., Ramaswamy, V., and Soden, B. J.: Tropospheric aerosol climate forcing in clear-sky satellite observations over the oceans, Science, 283, 1299–1303, 1999.
Hess, A. M., Koepke, P., and Schult, I.: Optical properties of aerosol and clouds: the software package OPAC, Bull. Am. Meteorol. Soc., 79, 831–844, 1998.
Holben, B. N., Eck, T. F., Slutsker, I. et al.: AERONET–A federated instrument network and data archive for aerosol characterization, Remote Sens. Environ., 66, 1–16, 1998.
Junge, C. E.: The size distribution and aging of natural aerosols as determined from electrical and optical measurements in the atmosphere, J. Meteorol., 12, 13–25, 1955.
Kalapureddy, M. C. R. and Devara, P. C. S.: Characterization of aerosols over oceanic regions around India during pre-monsoon 2006, Atmos. Environ., 42, 6816–6827, doi:10.1016/j.atmosenv.2008.05.022, 2008.
Kalapureddy, M. C. R., Ernest Raj, P., and Devara, P. C. S.: Total column ozone variations over oceanic region around Indian sub-continent during pre-monsoon of 2006, Atmosph. Chem. Phys. Discus., 8, 3143–3162, 2008.
Kaskaoutis, D. G. and Kambezidis, H. D.: Investigation on the wavelength dependence of the aerosol optical depth in the Athens area, Q. J. R. Meteorol. Soc., 132, 2217–2234, 2006.
Kaskaoutis, D. G., Kambezidis, H. D., Adamopoulos, A. D., and Kassomenos, P. A.: Comparison between experimental data and modeling estimates of atmospheric optical depth over Athens, Greece, J. Atmos. Solar Terr. Phys., 68, 1167–1178, 2006.
Kaskaoutis, D. G., Kambezidis, H. D., Hatzianastassiou, N., Kosmopoulos, P. G., and Badarinath, K. V. S.: Aerosol climatology: dependence of the Angstrom exponent on wavelength over four AERNET sites, Atmosph. Chem. Phys. Discus., 7, 7347–7397, 2007a.
Kaskaoutis, D. G., Kambezidis, H. D., Shailesh Kumar Kharol, and Badarinath, K. V. S.: Investigation on the ozone and trace gases contribution to the total optical depth in a polluted urban environment, Atmos. Res., 86, 286–296, 2007b.

Kaskaoutis, D. G. and Kambezidis, H. D.: Comparison of the Ångström parameters retrieval in different spectral ranges with the use of different techniques, Meteorol. Atmos. Phys., 99, 233–246, 2008.
King, M. D. and Byrne, D. M.: A method for inferring total ozone content from spectral variation of total optical depth obtained with a solar radiometer, J. Atmos. Sci., 33, 2242–2251, 1976.
Krishnamurti, T. N., Jha, B., Prospero, J., Jayaraman, A., and Ramanathan, V.: Aerosol and pollutant transport and their impact on radiative forcing over the tropical Indian Ocean during the January-February 1996 pre-INDOEX cruise, Tellus, 50B, 521–542, 1998.
Kumar, A., Sarin, M. M., and Sudheer, A. K.: Mineral and anthropogenic aerosols in Arabian Sea-atmosphere boundary layer: Sources and spatial variability, Atmos. Environ., 42, 5169–5181, doi:10.1016/j.atmosenv.2008.03.004, 2008.
Li, F. and Ramanathan, V.: Winter to summer monsoon variation of aerosol optical depth over the tropical Indian Ocean, J. Geophys. Res., 107, 4284, doi:10.1029/2001JD000949, 2002.
Madhavan, B.L., Niranjan, K., Sreekanth, V., Sarin, M.M., and Sudheer, A.K.: Aerosol characterization during the summer monsoon period over a tropical coastal Indian station, Visakhapatnam, J. Geophys. Res., 113, D21208, doi:10.1029/2008JD010272, 2008.
Moorthy, K. K. et al.: Aerosol climatology over India: 1. ISRO GBR MWR network and database, ISRO GBR SR-03-99, Indian Space Res. Organ., Bangalore, 1999.
Moorthy, K. K. and Satheesh, S. K.: Characteristics of aerosols over a remote island, Minicoy in the Arabian Sea: optical properties and retrieved size characteristics, Q. J. R. Meteorol. Soc., 126, 81–109, 2000.
Moorthy, K. K., Babu, S. S., and Satheesh, S. K.: Aerosol characteristics and Radiative Impacts over the Arabian Sea during the Intermonsoon Season: Results from the ARMEX field campaign, J. Atmos. Sci., 62, 192–206, 2005.
Moorthy, K. K., Satheesh, S. K., Babu, S. S., and Dutt, C. B. S.: Integrated Campaign for Aerosols, gases and Radiation Budget (ICARB): An overview, J. Earth System Sci., 117, S1, 243–262, 2008.
Morys, M., Mims III, F. M., Hagerup, S., Anderson, S. E., Baker, A., Kia, J., and Walkup, T.: Design, calibration, and performance of MICROTOPS II handheld ozone monitor and sun photometer, J. Geophys. Res., 106, 14 573–14 582, 2001.
Nair, P. R., Parameswaran, K., Sunil Kumar, S. V., Rajan, R.: Continental influence on the spatial distribution of particulate loading over the Indian Ocean during winter season, J. Atmos. Solar Terr. Phys., 66, 27–38, 2004.

Nair, V. S., Moorthy, K. K., and Babu, S. S.: Size segregated aerosol mass concentration measurements over the Arabian Sea during ICARB, J. Earth System Sci.,, 117, 315–323, 2008.
O'Neill, N. T., Dubovic, O., and Eck, T. F.: Modified Ångström exponent for the characterization of submicrometer aerosols, Appl. Opt., 40, 2368–2375, 2001.
Quinn, P. K., Coffman, D. J., Bates, T. S., Miller, T. L., Johnson, J. E., Welton, E. J., Neusüss, C., Miller, M., and Sheridan, P .J.: Aerosol optical properties during INDOEX 1999:Means, variability, and controlling factors, J. Geophys. Res., 107, 8020, doi:10.1029/2000JD000037, 2002.
Ramachandran, S. and Jayaraman, A.: Premonsoon aerosol loading and size distribution over the Arabian Sea and the Tropical Indian Ocean, J. Geophys. Res., 107, 4738, doi:10.1029/2002JD002386, 2002.
Ramachandran, S.: Spectral aerosol optical characteristics during the northeast monsoon over the Arabian Sea and the tropical Indian Ocean: 1. Aerosol optical depths and their variabilities, J. Geophys. Res., 109, D19207, doi:10.1029/2003JD004476, 2004a.
Ramachandran, S.: Spectral aerosol optical characteristics during the northeast monsoon over the Arabian Sea and the tropical Indian Ocean: 2. Angstrom and anthropogenic influence, J. Geophys. Res., 109, D19208, doi:10.1029/2003JD004483, 2004b.
Reid, J. S., Eck, T. F., Christopher, S. A., Hobbs, P. V., and Holben, B. N.: Use of the Angstrom exponent to estimate the variability of optical and physical properties of aging smoke particles in Brazil, J. Geophys. Res., 104, 27473–27489, 1999.
Satheesh, S. K., Ramanathan, V., Jones, L. X., Lobert, J. M., Podrogny, I. A., Prospero, J. M., Holben, B. N., and Loeb, N. G.: A model for the natural and anthropogenic aerosols for the tropical Indian Ocean derived from Indian Ocean experiment data, J. Geophys. Res., 104, 27421–27440, 1999.
Satheesh, S. K., Ramanathan, V., Holben, B. N., Moorthy, K. K., Loeb, N. G., Maring, H., Prospero, J. M., and Savoie, D.: Chemical, microphysical, and radiative effects of Indian Ocean aerosols, J. Geophys. Res., 107, 4725, doi:10.1029/2002JD002463, 2002.
Satheesh, S. K., Moorthy, K. K., Kaufman, Y. J., and Takemura, T.: Aerosol optical depth, physical properties and radiative forcing over the Arabian Sea, Meteorol. Atmos. Phys., 91, 45–62, 2006a.
Satheesh, S. K., Srinivasan, J., and Moorthy, K. K.: Contribution of sea-salt to aerosol optical depth over the Arabian Sea derived from MODIS observations, Geophys. Res. Lett., 33,

L03809, doi:10.1029/2005GL024856, 2006b.
Savoie, D. L., Prospero, J. M., and Nees, R. T.: Nitrate, non-sea-salt sulfate, and mineral aerosol over the northwestern Indian Ocean, J. Geophys. Res., 92, 933–942, 1987.
Schuster, G. L., Dubovik, O., and Holben, B. N.: Angstrom exponent and bimodal aerosol size distributions, J. Geophys. Res., 111, D07207, doi:101029/2005JD006328, 2006.
Shaw, G. E.: Absorption continuum in the near IR near 1 μm, Appl. Opt., 19, 480–482, 1980.
Smirnov, A., Holben, B. N., Kaufman, Y. J., Dubovic, O., Eck, T. F., Slutsker, I., Pietras, C., and Halthore, R. N.: Optical properties of atmospheric aerosol in Maritime Environments, J Atmos. Sci., 59, 501–523, 2002.

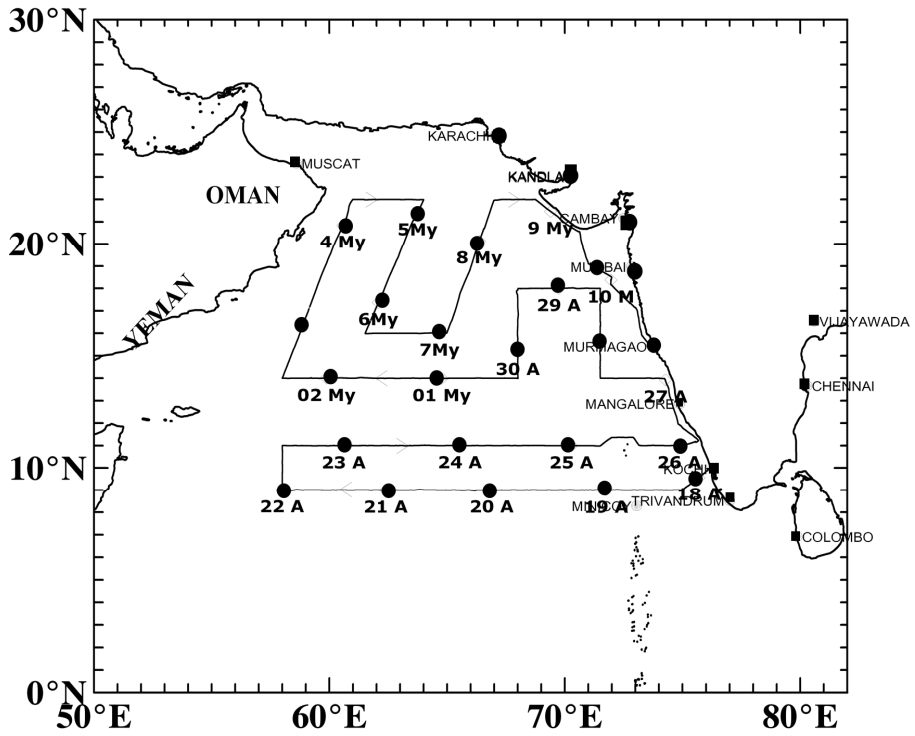

Fig. 1. The cruise legs (solid lines) of the Sagar Kanya 223B in the Arabian Sea in the period 18 April–10 May 2006 with indications of the daily position of the ship at 05:30 UTC denoted by the circles. The major ports and coastal urban centers on the mainland adjoining the cruise track are also identified. The date at each position also indicated (A=April, My=May).

ACPD
9, 22223–22269, 2009

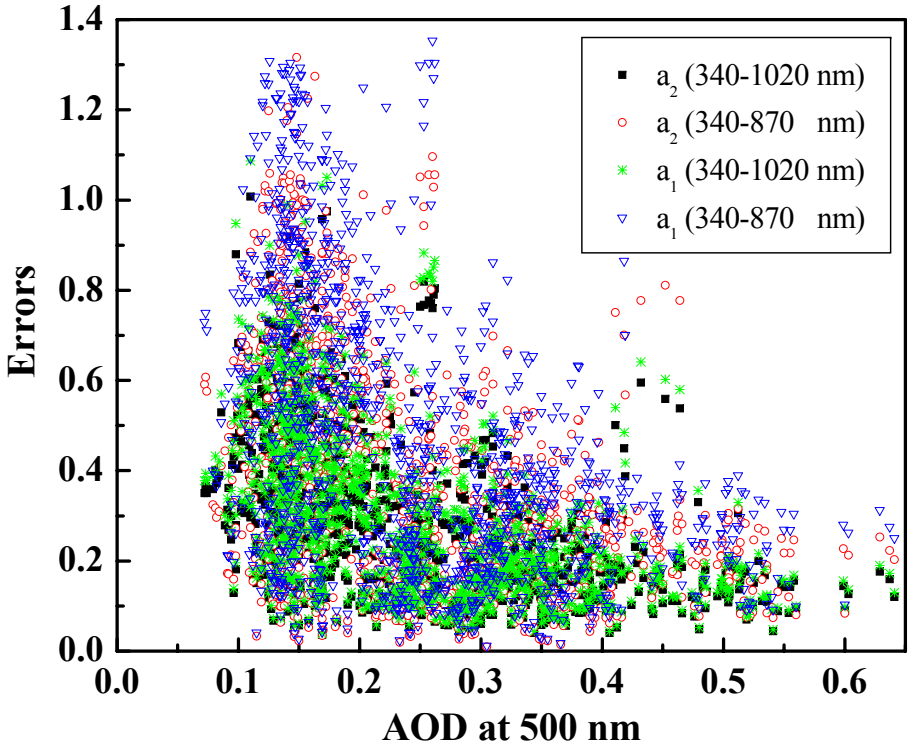

Fig. 2. Correlation of the standard error with the AOD_{500} values. The errors in both a_1 and a_2 obtained from the polynomial fit of the $\ln\tau_\alpha$ vs. $\ln\lambda$.

ACPD
9, 22223–22269, 2009

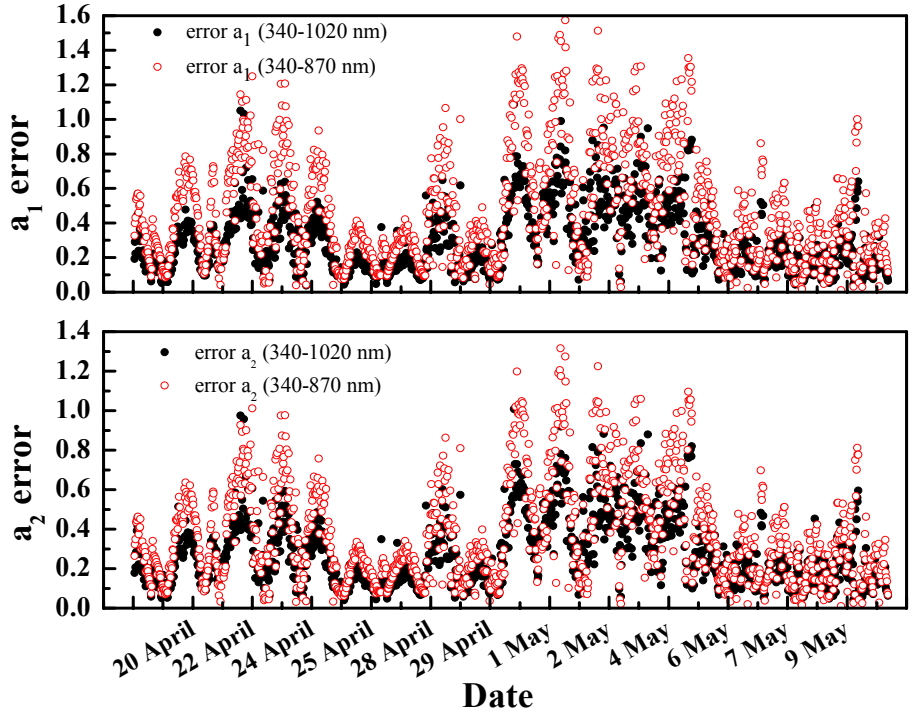

Fig. 3. Day-to-day variation of the a_1 (upper panel) and a_2 (lower panel) typical errors.

ACPD
9, 22223–22269, 2009

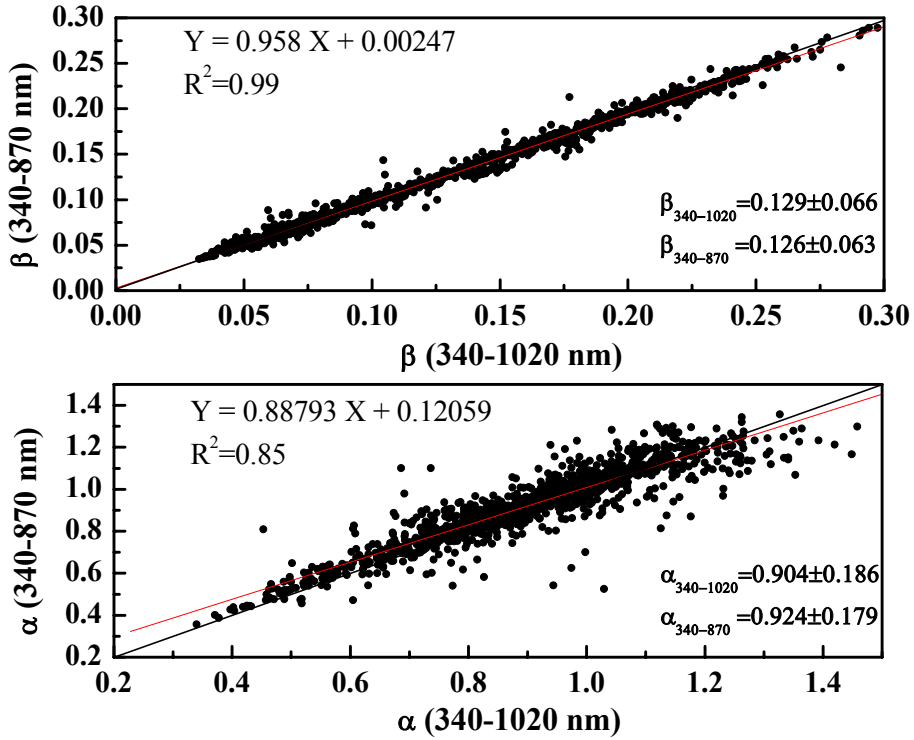

Fig. 4. Correlation between the Ångström parameters α and β in two different spectral bands. The black line represents the y = x condition and the red line the linear equation shown in the graph.

ACPD
9, 22223–22269, 2009

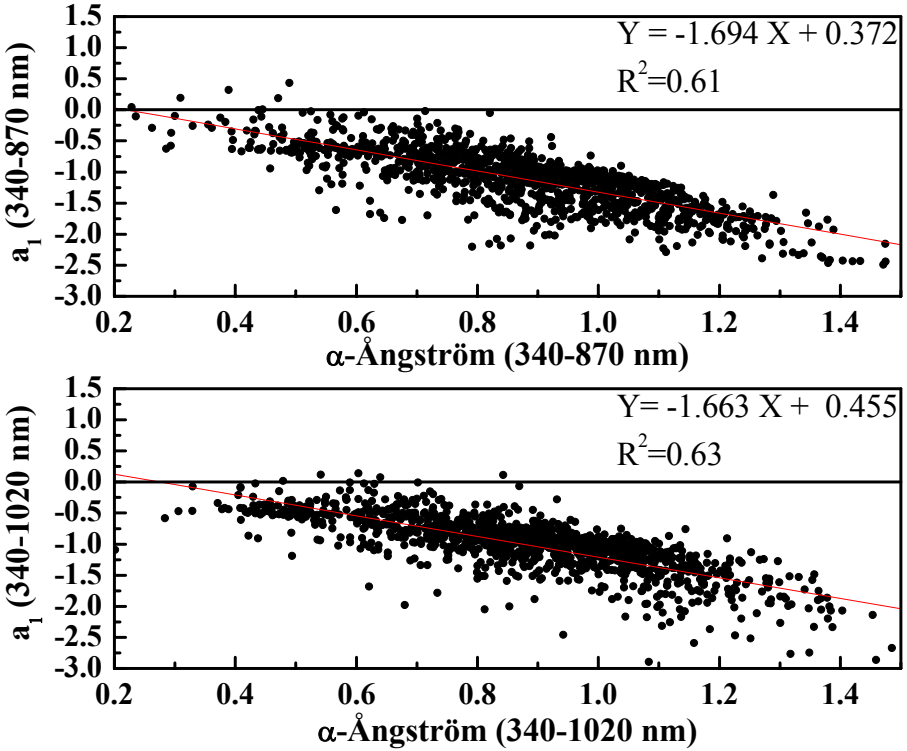

Fig. 5. Correlation between α and a_1 in two different spectral bands. The red line represents the linear equation given in the graph.

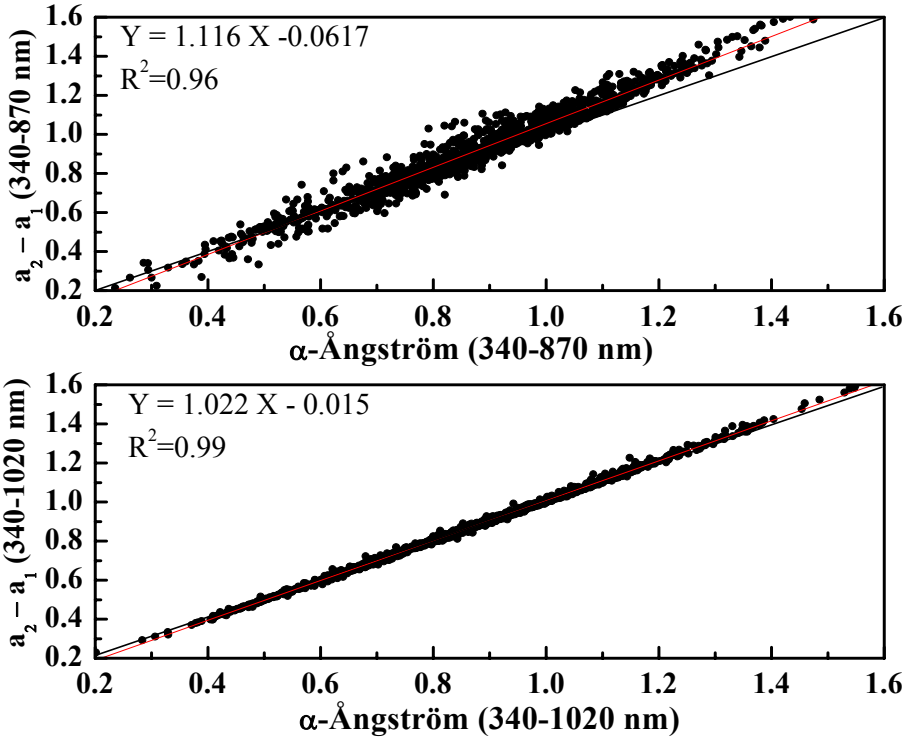

Fig. 6. Correlation between the differences a_2–a_1 and the α values in two different spectral bands. The black lines represents the y-x condition and the red line the linear equation given in the graph.

ACPD
9, 22223–22269, 2009

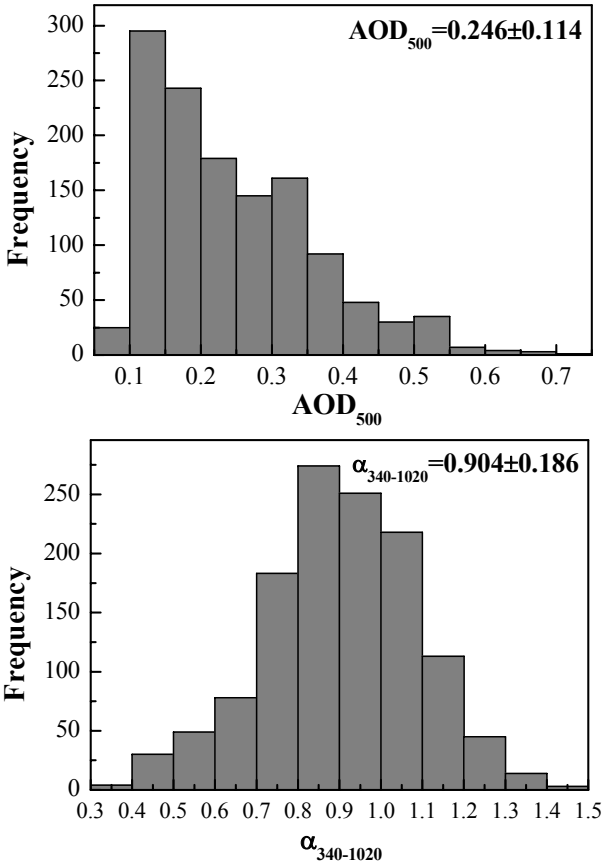

Fig. 7. Histograms of the number of cases for the AOD_{500} (upper panel) and $\alpha_{340-1020}$ (lower panel) in the AS during the period 18 April–10 May 2006. The given values in the graphs are the mean ones and their standard deviations over the entire experimental period.

ACPD
9, 22223–22269, 2009

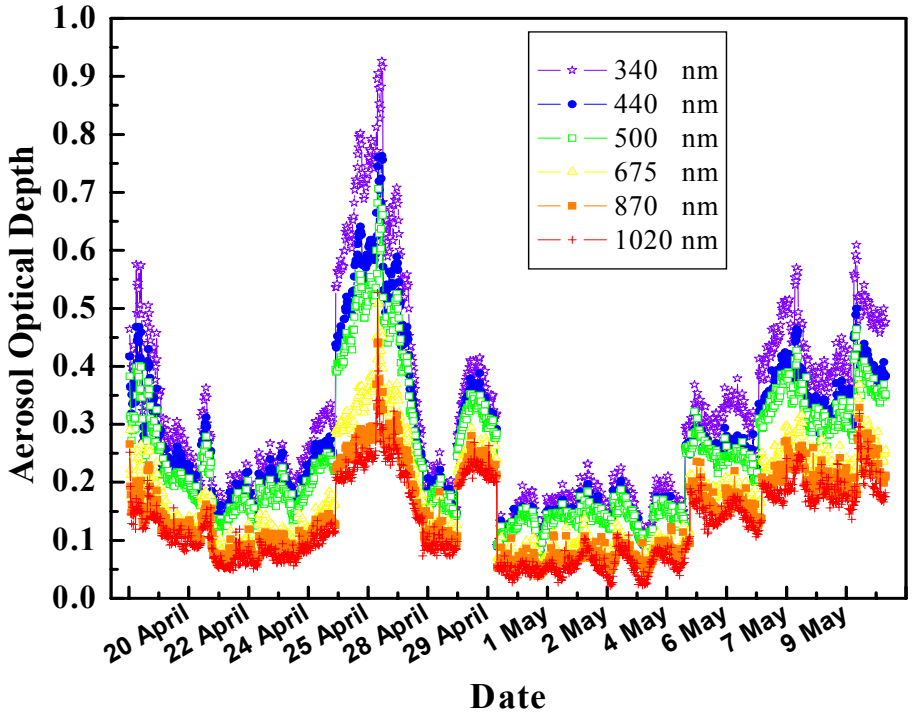

Fig. 8. Temporal variation of the spectral AOD in the AS during the ICARB campaign.

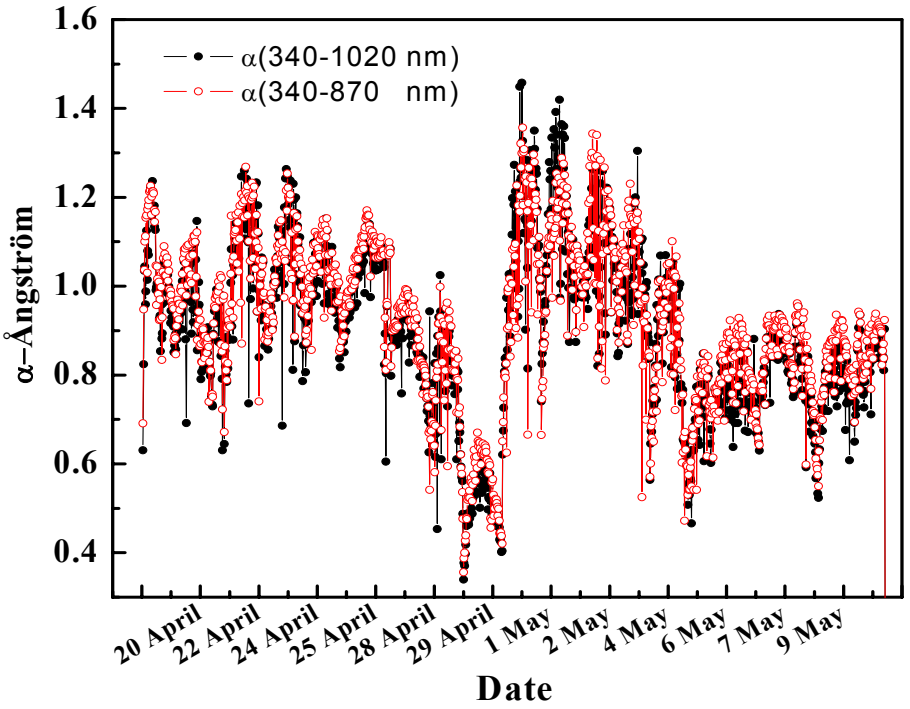

Fig. 9. Same as in Fig. 8, but for the Ångström exponent α in two different spectral bands, black for 340–1020 nm and red for 340–870 nm.

ACPD
9, 22223–22269, 2009

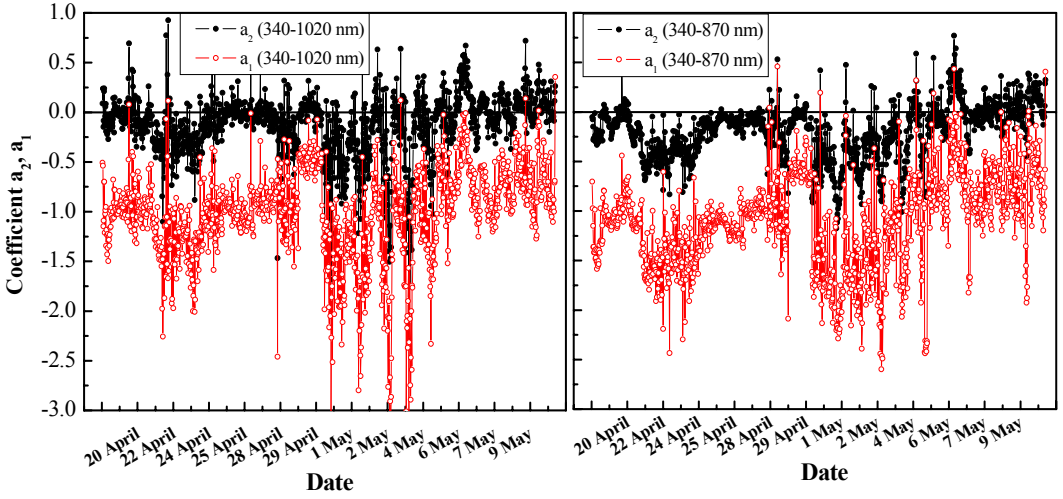

Fig. 10. Same as in Fig. 8, but for the coefficients a_1 and a_2 (Eq. 2) calculated in (left) the 340–1020-nm spectral band, (right) the spectral band of 340–870 nm.

ACPD
9, 22223–22269, 2009

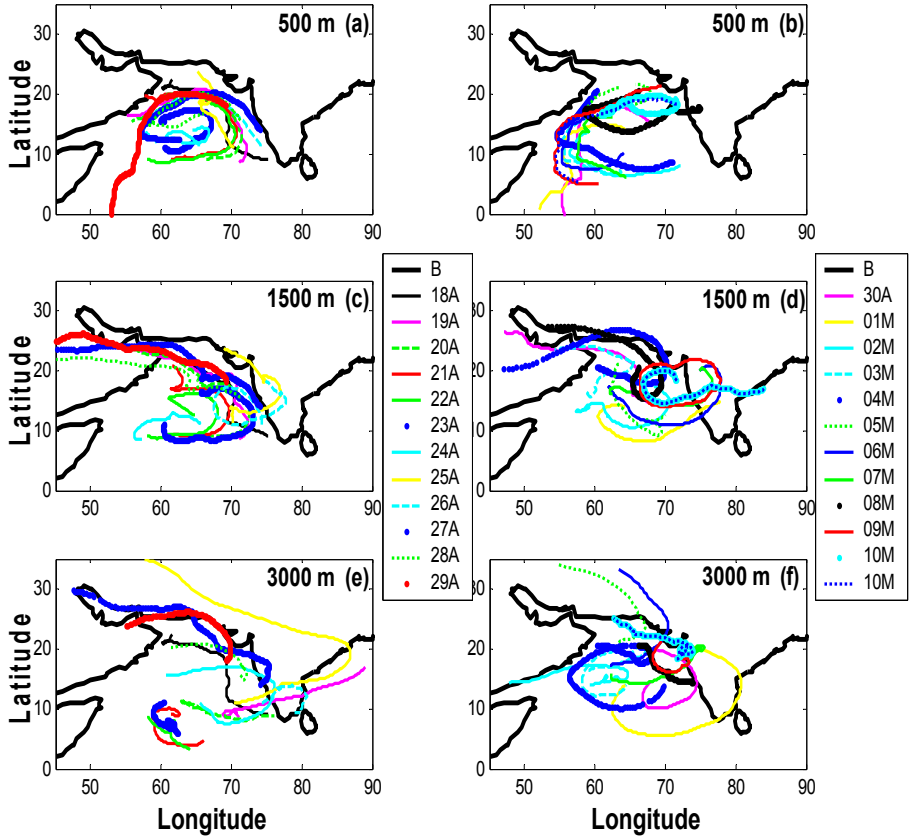

Fig. 11. 7-day back trajectories from the HYSPLIT model ending on at altitudes **(a–b)** 500 m, **(c–d)** 1500 m and **(e–f)** 3000 m.

ACPD
9, 22223–22269, 2009

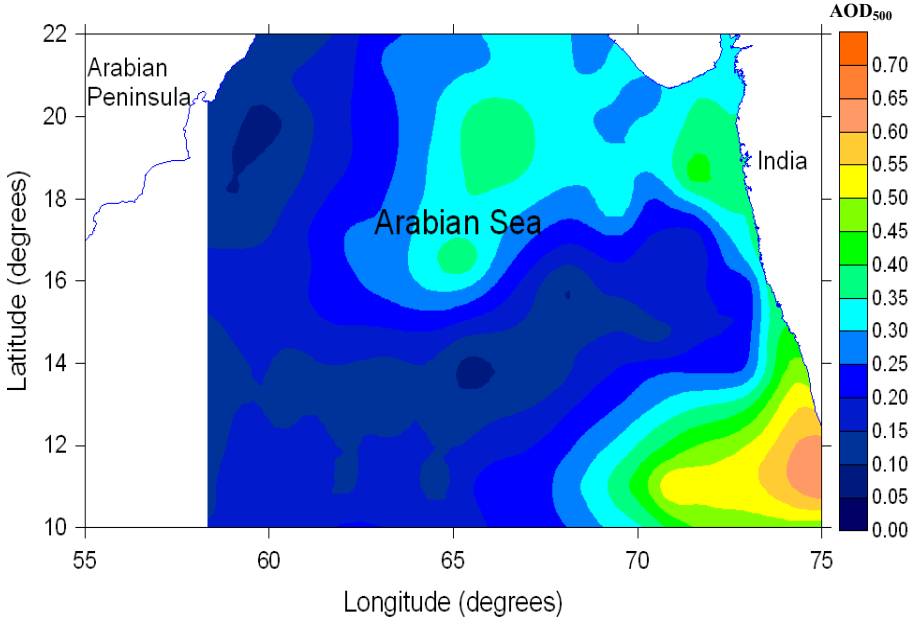

Fig. 12. Spatial distribution of the AOD_{500} values regarding the whole set of measurements over the AS region.

ACPD
9, 22223–22269, 2009

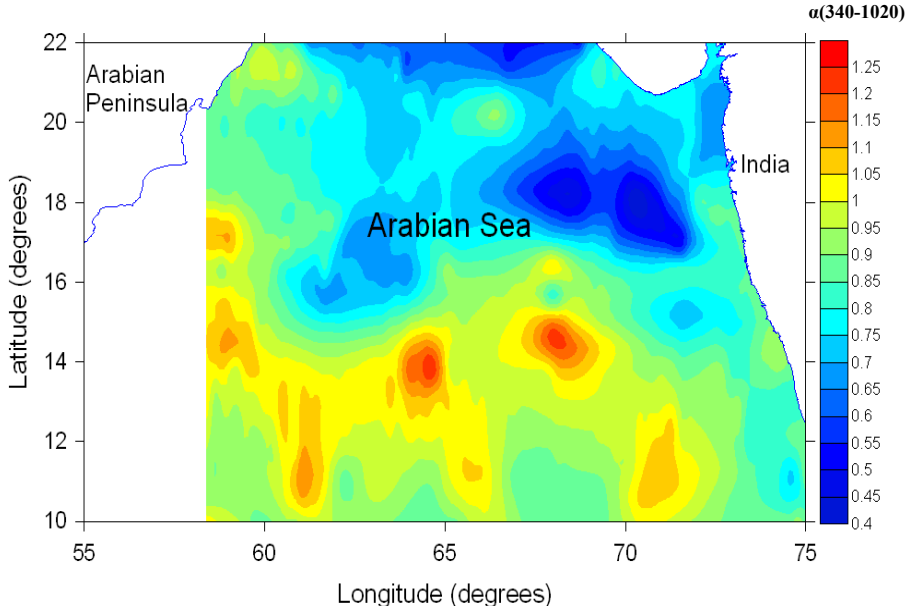

Fig. 13. Same as in Fig. 12, but for the $\alpha_{340-1020}$.

ACPD
9, 22223–22269, 2009

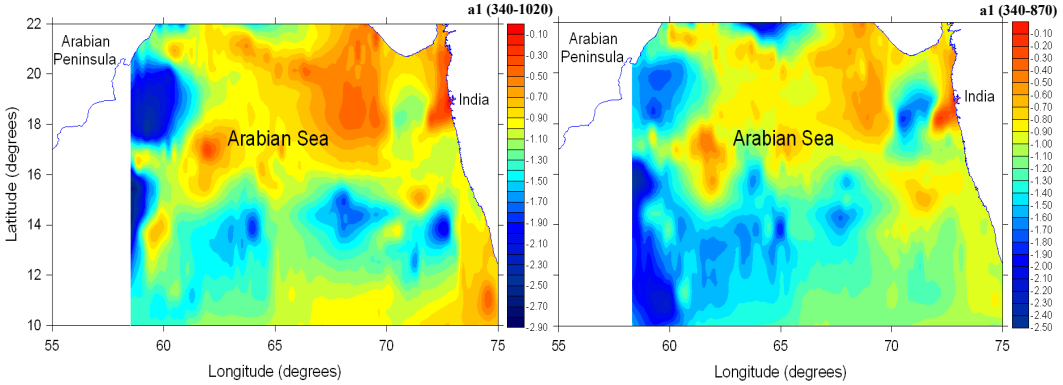

Fig. 14. Spatial distribution of the a_1 values regarding the whole set of measurements over the AS region computed in the 340–1020-nm band (left) and the 340–870-nm band (right).

ACPD
9, 22223–22269, 2009

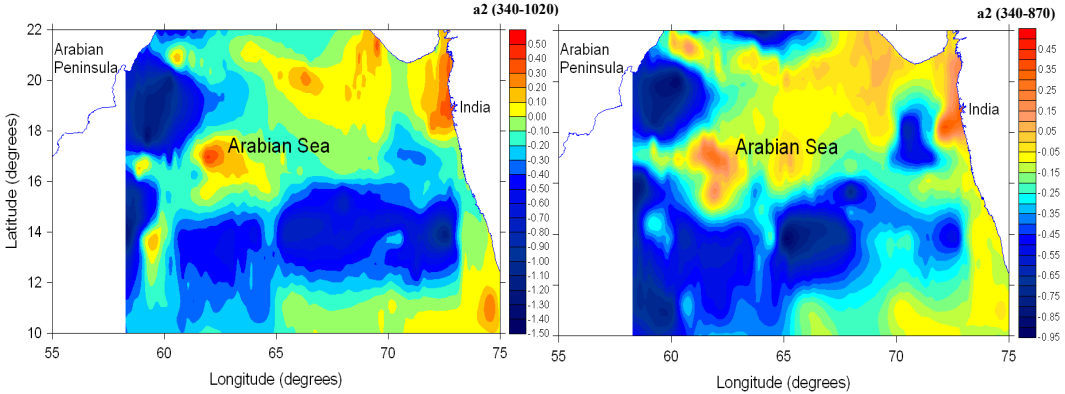

Fig. 15. Same as Fig. 14, but for the a_2 values.

ACPD
9, 22223–22269, 2009